This manuscript is a non-peer-reviewed preprint submitted to OSF Preprints. It will be submitted to a geophysics-related journal.

A Robust Geometric Factor for 3D ERT Based on a Field-Aligned Approach

Churl Hyun Jo

Subsurface Information Technologies, Inc., Republic of Korea. E-mail: chjo@geeha.co.kr

ABSTRACT

Apparent resistivity is a fundamental concept in electrical resistivity tomography (ERT), governed by the geometric factor. For non-collinear electrode configurations, especially in 3D surveys, a more consistent and robust formulation of the geometric factor is needed. We propose a generalized method using field-aligned virtual points—theoretical positions aligned with the electric field direction in a homogeneous half-space. These points are defined on a circle centered at the midpoint of a potential electrode pair, allowing the geometric factor to be formulated independently of electrode alignment. This method yields apparent resistivity values consistent with the true resistivity under homogeneous conditions, except near current electrodes where electric field curvature is significant. The proposed framework extends naturally to arbitrary and highly non-collinear electrode configurations, providing a robust foundation for apparent resistivity calculations in 3D ERT.

Keywords: 3D ERT, non-collinear electrode configurations, apparent resistivity, field-aligned virtual points, geometric factor

INTRODUCTION

Apparent resistivity is a fundamental concept in electrical resistivity tomography (ERT). It converts the measured voltage differences, which depend on electrode geometry, into a physically meaningful parameter that serves as an interface between data acquisition, quality control, interpretation, and inversion. According to Parasnis (1975), apparent resistivity is essentially a formal concept; in terms of measurable quantities, it represents a standardized voltage difference. In other words, apparent resistivity is not the only conceivable way to standardize voltage measurements. However, its unique property—coinciding with the true resistivity in a homogeneous medium—makes it a particularly useful and practical standardization scheme. For this reason, apparent resistivity continues to play a central role in data processing and interpretation.

ERT has been widely applied in near-surface geophysics and mineral exploration, most often using 2D models. In this framework, the basic electrode arrays are typically collinear. In this case, the definition of the geometric factor required for computing apparent resistivity is straightforward. In contrast, for 3D surveys, non-collinear electrode arrangements can be encountered not only when survey lines cannot be kept straight due to topographic obstacles or logistical constraints. They also arise when

the target structures are highly irregular in shape and exhibit strong conductivity contrasts with the background medium (Jo, 2025). In such cases, the definition of the geometric factor has not yet been systematically established or universally accepted.

In earlier studies, Bibby and Risk (1973) considered dipole–dipole arrays in geothermal exploration, where the total electric field was measured. Keller et al. (1975) introduced the bipole–dipole (dipole mapping) method, in which apparent resistivity could be defined from different electric-field components. Both studies proposed definitions of the geometric factor to compute apparent resistivity, but their formulations lacked a unified principle and were often overly complex for intuitive understanding.

In this study, we revisit the problem of defining geometric factors for cases arising in 3D ERT, particularly when measuring the total electric field or when survey lines deviate from straight alignment. Our aim is to derive a generalized expression of apparent resistivity that remains consistent under such conditions. A key consideration is that the geometric factors traditionally defined for 2D ERT implicitly assumed collinearity of current and potential electrodes. This assumption ensured that the survey line coincided not only with the electrode alignment but also with the electric field direction in a homogeneous medium—although this equivalence was rarely emphasized. We argue that, more fundamentally, the reference points used in defining geometric factors should be aligned with the electric field direction. Building on this perspective, we propose a generalized approach to apparent resistivity that incorporates field-aligned reference positions, ensuring consistent standardization beyond collinear configurations.

ROBUST FORMULATION OF THE GEOMETRIC FACTOR

Electric field in a homogeneous medium

In a homogeneous, isotropic half-space, the potential V at a point P due to a current dipole (C1, C2; with C2 as source and C1 as sink) is expressed as

$$V(P) = \frac{\rho_0 I}{2\pi}\left(\frac{1}{R_{PC2}} - \frac{1}{R_{PC1}}\right), \tag{1}$$

where I is the injected current, ρ_0 is the medium resistivity, and R_{AB} denotes the distance between points A and B. The associated electric field is the negative gradient of the potential,

$$\boldsymbol{E}(P) = -\nabla V(P). \tag{2}$$

In this formulation, the resistivity ρ_0 and the current I act only as multiplicative scaling factors. By contrast, in a homogeneous isotropic medium, the direction of the electric field vectors is determined solely by the geometry of the current electrodes, independent of resistivity or current strength (see, e.g.,

Telford et al., 1990). Thus, once the current dipole is specified, the induced field direction remains invariant, independent of ρ_0 or I.

This invariant directional field pattern, hereafter referred to as the *primary field*, is illustrated in Figure 1 with equipotential contours and field vectors. An enlarged view (Figure 2) further clarifies that, for collinear configurations, the field direction coincides with the straight line connecting the two current electrodes, whereas off-line points reveal deviations that align perpendicularly to the local equipotential contours. These observations establish a physical basis for defining potential measurements in terms of the local field direction. In this context, *virtual points* aligned with the electric field direction (shown as blank diamonds in Figure 2) provide the reference positions used in formulating a robust geometric factor.

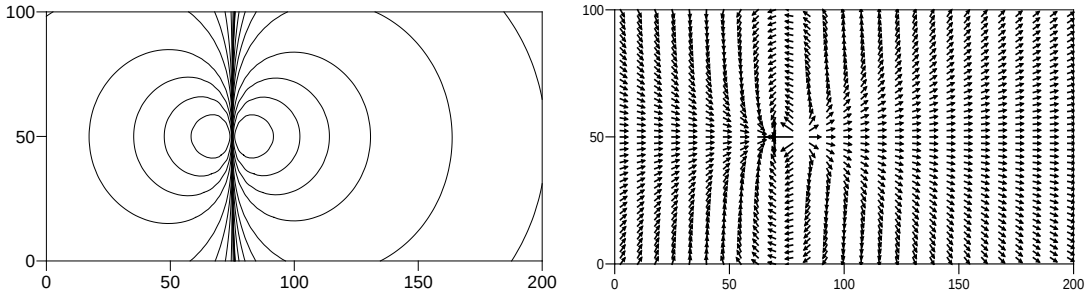

(a) (b)

Figure 1. Electric field generated by a current dipole in a homogeneous half-space model. The source and sink poles are located at (80, 50) and (70, 50), respectively. (a) Equipotential contours at the surface. (b) Vector plot of the electric field distribution.

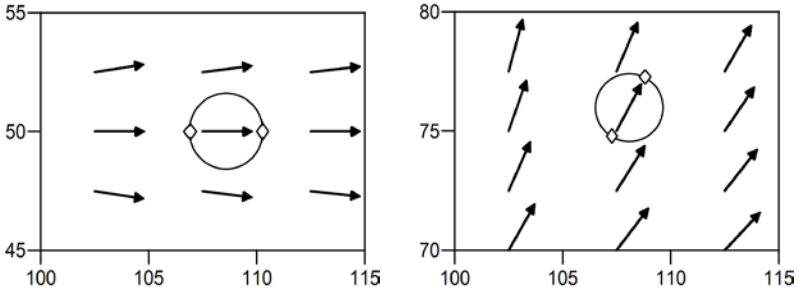

(a) (b)

Figure 2. Enlarged view of the electric field directions from Figure 1b. Blank diamonds denote the field-al igned virtual points used to define the geometric factor. (a) At points along the line connecting the two cu rrent electrodes, the field direction coincides with this line. (b) At an off-line point, the field direction devi ates and instead aligns perpendicularly to the local equipotential contours.

Redefining potential-difference measurement

Let us reconsider the basis of potential-difference measurements in ERT. In the widely used collinear arrays, the survey line is aligned with the straight line connecting the two current electrodes, and the electric field is assumed to be directed solely along this line. The potential difference is then measured between two electrodes placed symmetrically at a distance of $dx/2$ from the midpoint of the potential pair, where dx is the electrode spacing.

When extended to 3D, a more general framework is required. For the common case in which the measurement plane is the ground surface, the electric field has two horizontal components, and thus its magnitude and direction must be determined using two linearly independent potential-difference pairs. A practical approach is to place two mutually perpendicular electrode pairs on a circle of radius $dx/2$, centered at the *potential-measurement reference point* (i.e., the midpoint of the potential electrode pair) (Figure 3).

From this consideration, we propose a revised definition of potential-difference measurement in electrical prospecting: the measurement is taken between an electrode pair located at antipodal points on a circle centered at the potential-measurement reference point, with radius equal to half the electrode spacing, $dx/2$. We hereafter refer to this construction as the *potential-difference measurement circle*. This definition provides the basis for consistently treating potential differences in both collinear and non-collinear configurations.

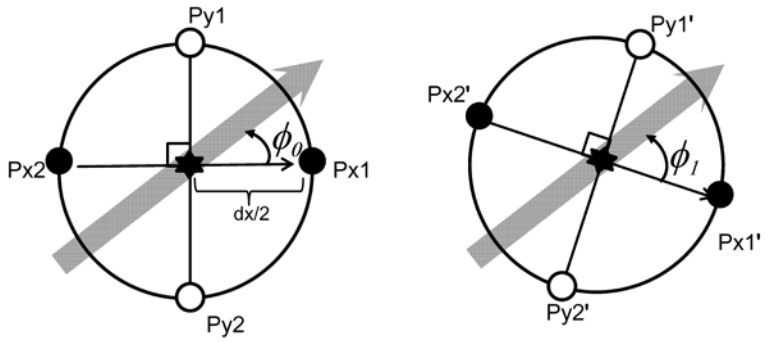

(a) (b)

Figure 3. (a) Definition of the potential-difference measurement circle with radius dx/2. Two mutually per pendicular potential-electrode pairs (*Px1–Px2* and *Py1–Py2*) are shown. (b) Rotated electrode pairs illustr ating that any orthogonal configuration on the same circle (*dx*/2) can be used to resolve the field magnitud e and direction.

Primary-field direction in a homogeneous medium

Building on the above conceptual framework, we now formalize the determination of the primary -field orientation at an arbitrary potential-difference center P at $(x_p,\ y_p)$. Let the negative and positive current electrodes be at C_1 $(x_{c1},\ y_{c1})$ and C_2 $(x_{c2},\ y_{c2})$, respectively, and let r denote half the potential-electrode spacing, i.e., the radius of the potential-difference measurement circle. Then, two orthogonal ele ctrode pairs are defined on this circle for sampling the local field component,

$$P_{x1} = (x_p + r, y_p), P_{x2} = (x_p - r, y_p),\quad P_{y1} = (x_p, y_p + r), P_{y2} = (x_p, y_p - r). \tag{3}$$

The potential differences across the orthogonal pairs are

$$\Delta V_{Px} = \frac{I\rho_0}{2\pi}\left\{\left(\frac{1}{R_{P_{x1}C_2}} - \frac{1}{R_{P_{x1}C_1}}\right) - \left(\frac{1}{R_{P_{x2}C_2}} - \frac{1}{R_{P_{x2}C_1}}\right)\right\}, \tag{4}$$

$$\Delta V_{Py} = \frac{I\rho_0}{2\pi}\left\{\left(\frac{1}{R_{P_{y1}C_2}} - \frac{1}{R_{P_{y1}C_1}}\right) - \left(\frac{1}{R_{P_{y2}C_2}} - \frac{1}{R_{P_{y2}C_1}}\right)\right\}.$$

Using the finite-difference approximation over an interval of 2r, the local horizontal field components are

$$E_x \approx -\frac{\Delta V_{Px}}{2r},\quad \mathrm{E_y} \approx -\frac{\Delta V_{Py}}{2r}\ . \tag{5}$$

The primary-field orientation at P is obtained as

$$\theta_0 = atan2(E_y, E_x) \approx atan2(-\Delta V_{Py}, -\Delta V_{Px})\ . \tag{6}$$

This formal derivation connects the conceptual notion of the primary field with explicit electrode geometry.

Field-aligned virtual points on the potential-difference measurement circle

The two antipodal points lying on the potential-difference measurement circle along the local pri mary-field direction are given by,

$$P_{v1} = (x_p + r\cos\theta_0,\ y_p + r\sin\theta_0),\quad P_{v2} = (x_p - r\cos\theta_0, y_p - r\sin\theta_0). \tag{7}$$

We designate P_{v1} and P_{v2} as the *field-aligned virtual points* (*FAViPs*) at P. They may also simply be referr ed to as *principal points* in the context of formulating the robust geometric factor.

Robust geometric factor based on FAViPs

With these definitions, the robust geometric factor evaluated at P is

$$G = \left\{\left(\frac{1}{R_{P_{v1}C_2}} - \frac{1}{R_{P_{v1}C_1}}\right) - \left(\frac{1}{R_{P_{v2}C_2}} - \frac{1}{R_{P_{v2}C_1}}\right)\right\}^{-1}. \quad (8)$$

This definition reduces to the conventional collinear geometric factor when P_{v1} and P_{v2} coincide with the survey line connecting C_1 and C_2; more generally, it remains well-posed for arbitrary, non-collinear configurations because the FAViPs are constructed directly from the local primary-field direction at P.

Importantly, the robust factor defined in equation (8) can also be incorporated into data processing schemes that utilize horizontal vector measurements, such as the method proposed by Jo (2025).

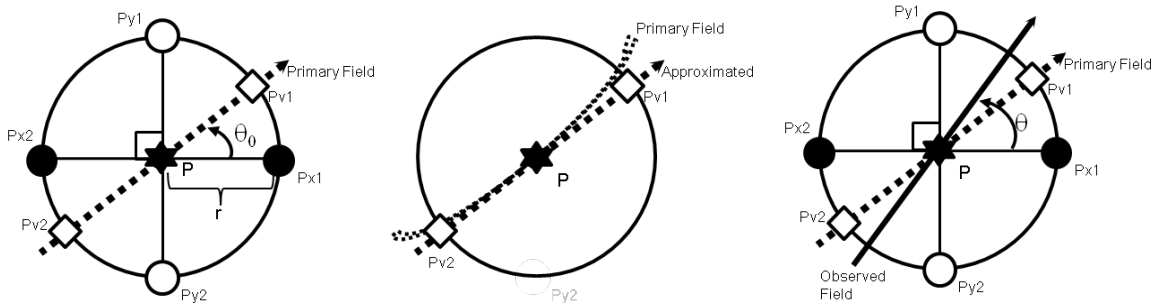

(a) (b) (c)

Figure 4. (a) The virtual points (P_{v1} and P_{v2}), aligned with the (approximated) primary field, used to define the robust geometric factor. (b) Schematic illustration of field curvature within the potential-difference measurement circle. The straight line connecting the virtual points represents the approximated field direction, whereas the curved arrows indicate the theoretical field direction. (c) The actual field can be measured using any two mutually perpendicular potential-electrode pairs as in Figure 3(b). In this example, the same electrode pairs that define the virtual points are used for the field measurement.

VERIFICATION OF THE ROBUST GEOMETRIC FACTOR

To verify the validity of the robust geometric factor, we tested whether the true resistivity can be recovered from two independent approaches using measured electric-field values. For consistency, the model configuration is identical to that shown in Figure 1. In this test, the potential-difference measurement was made with an electrode spacing (i.e., circle diameter) of 10 m, and the resistivity of the homogeneous medium is 1000 Ω·m.

The apparent resistivity under consideration is computed from the magnitude of the total electric field, ΔV_t , together with the robust geometric factor. At the potential-difference center P, the total field magnitude is

$$\Delta V_t = \Delta V = \sqrt{\left(\Delta V_{Px}{}^2 + \Delta V_{Py}{}^2\right)} \quad (9)$$

and the apparent resistivity is then given by

$$\rho_a = \frac{2\pi}{I} \Delta V_t G. \quad (10)$$

Analytical verification

First, an analytical check was performed. The horizontal components of the potential difference obtained from equation (4), combined with the robust geometric factor defined in equation (8), were substituted into equations (9) and (10). The resulting apparent resistivity values were normalized by the true resistivity and plotted as relative-error contours (Figure 5).

Figure 5a illustrates the case of an extended dipole–dipole array (equivalently, the exterior-potential configuration; "exterior PP" in Szalai and Szarka, 2008), using a dipole source with 10 m spacing. Figure 5b shows the case of an extended Schlumberger array (equivalently, the interior- potential configuration; "interior PP" in Szalai and Szarka, 2008), using a current-electrode separation of 200 m.

In both cases, relative errors are less than 1% over most of the survey area, except near the current electrodes where errors slightly exceed 10%. In practical ERT surveys, resistivity variations on the order of 10% are generally regarded as negligible.

These errors arise because, even in a homogeneous medium, the electric field lines exhibit curvature away from the line connecting the current electrodes (Figures 4b). The FAViPs (or principal points) proposed in this study assume a straight-line field direction through the center of the potential-difference circle. This approximation does not fully represent the finite curvature of the actual field, resulting in small but localized errors.

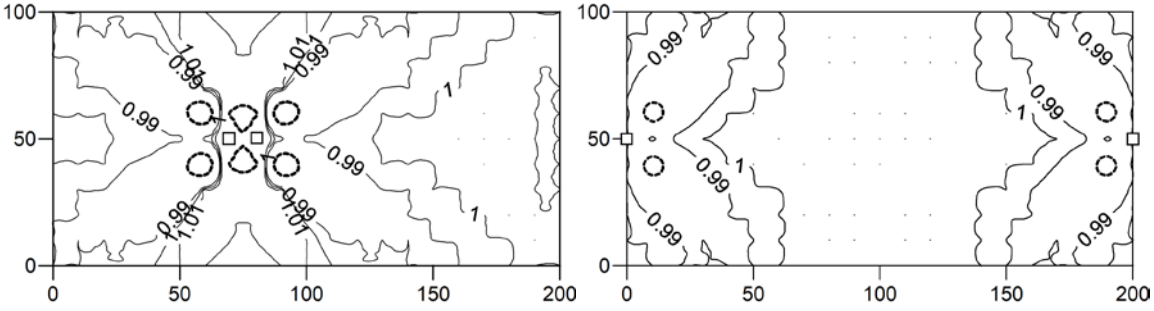

Figure 5. Relative error contours ρ_a/ρ_0 (calculated resistivity normalized by the true resistivity). Contour levels are set at ±1% and ±10% to emphasize error magnitudes; the ±10% contours are shown as dotted lines. Current electrode locations are marked by open squares. (a) Extended dipole–dipole source. (b) Extended Schlumberger (interior potential) source

Numerical verification

Second, numerical modeling was carried out to compute apparent resistivity values directly, following the same approach as above. Simulations were conducted for both extended dipole–dipole (exterior-potential) and extended Schlumberger (interior-potential) arrays. The modeling parameters are summarized in Table 1. The survey line layouts used for these simulations are shown in Figure 6.

Figure 7 presents apparent-resistivity values calculated from 3D FDM numerical modeling using the generalized geometric factors. In Figure 7a, the results for extended dipole–dipole arrays are plotted as functions of dipole spacing n. Except for n = 1 and 2, the apparent-resistivity values for all lines fall in the range of 950–980 Ω·m, corresponding to errors of less than 5% relative to the true resistivity. In Figure 7b, the results for the extended Schlumberger array are shown as functions of the potential-measurement position. To avoid locations too close to the current electrodes, the measurement ranges were restricted to x = 20–180 m for SD50 and x = 10–190 m for SD60, while for the other lines the full range x = 0–200 m was used. Excluding these near-source regions within 20 m of each current electrode, the apparent-resistivity values are mostly within about 10% of the true resistivity.

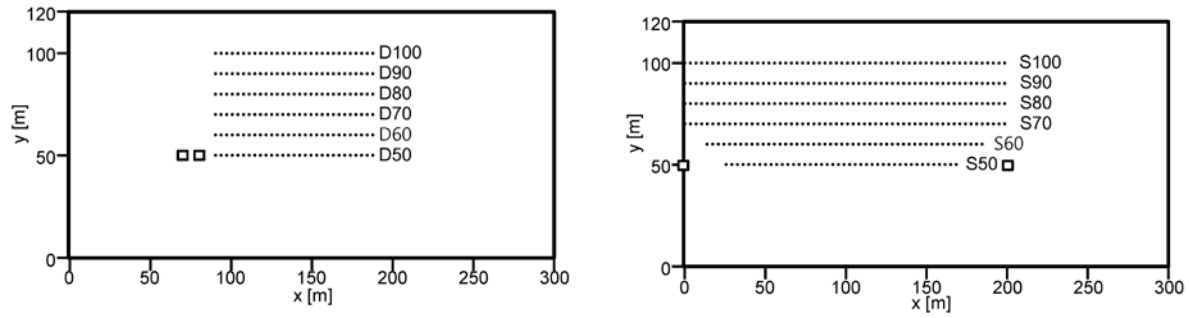

(a) (b)

Figure 6**.** Schematic diagrams of survey line layouts used for numerical calculation of apparent resistivity. Current-electrode positions are indicated by squares, and potential-electrode ranges by dotted lines. (a) Extended dipole–dipole array. (b) Extended Schlumberger array.

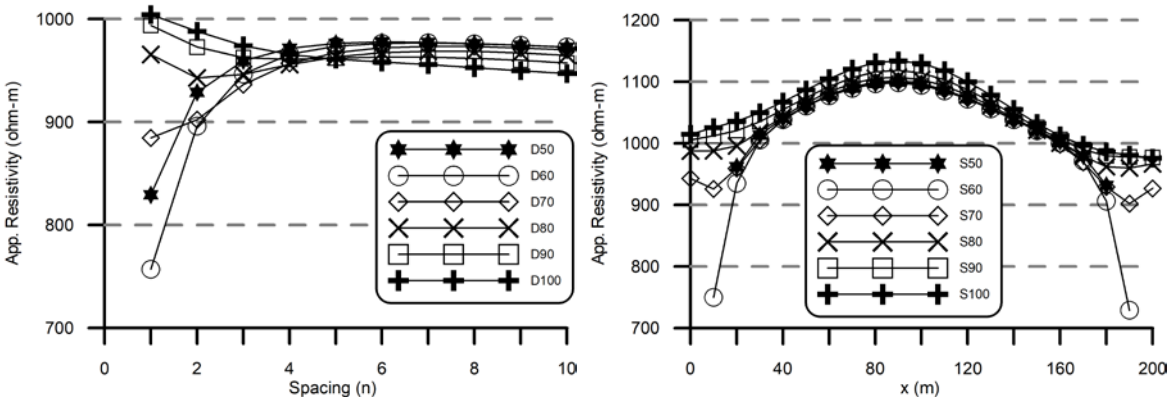

(a) (b)

Figure 7. Numerically calculated apparent resistivity using the generalized geometric factors. (a) Results for the extended dipole–dipole arrays. (b) Results for the extended Schlumberger array

Table 1. Numerical modeling parameters used in the verification test.

Parameter	Value / Description
Numerical method	3D finite-difference method (FDM)
Solver	Conjugate gradient; relative tolerance = 5×10^{-6}; no pre-Conditioner
Grid size	Nx = 121, Ny = 49, Nz = 49 (with 4 padding layers at all boundaries except surface)
Grid spacing	2.5 m (uniform); padding spacing increases outward by factors of 2, 4, 8, and 16
Host medium resistivity	1000 Ω·m

CONCLUSION

In this study, we proposed a generalized framework for defining the geometric factor in 3D ERT, based on the concept of field-aligned virtual points (FAViPs). These points are determined from the local primary-field direction in a homogeneous medium and provide a physically consistent basis for formulating apparent resistivity, even in non-collinear electrode configurations.

The analytical derivation showed that the robust geometric factor reduces to the conventional definition for collinear arrays while remaining valid for arbitrary geometries. Verification using both analytical calculations and 3D numerical modeling demonstrated that apparent resistivity values derived with the robust geometric factor generally match the true resistivity, with deviations remaining within about 10% except in the immediate vicinity of the current electrodes. Such localized discrepancies arise from the intrinsic curvature of electric-field lines, which cannot be fully represented by the straight-line

approximation of FAViPs, but the magnitude of these errors is generally minor and unlikely to affect practical ERT surveys.

The proposed approach provides a robust and unified scheme for apparent resistivity calculation, overcoming limitations of previous definitions that were restricted to collinear arrays. By enabling consistent treatment of non-collinear survey geometries, this framework offers potential benefits for survey design, data standardization, and inversion workflows in 3D ERT. Future work should focus on applying the method to field data, including cases that incorporate horizontal vector measurements, and on exploring its potential impact on inversion robustness and imaging resolution.

REFERENCES

Bibby, H. M., and Risk, G. F., 1973, Interpretation of dipole-dipole resistivity surveys using a hemispheroidal model, *Geophysics*, **38**, 719-736.

Jo, C. H., 2025, A horizontal vector approach to 3D electrical resistivity tomography, EarthArXiv, https://doi.org/10.31223/X52J0J.

Keller, G. V., Furgerson, R., Lee, C. Y., Harthil, N., and Jacobson, J. J., 1975, The dipole mapping method, *Geophysics*, **40**, 451-472.

Parasnis, D.S., 1975, *Mining Geophysics*, Elsevier, 174 pp.

Szalai, S., and Szarka, L., 2008, On the classification of surface geoelectric arrays, *Geophysical Prospecting*, **56**, 159–175.

Telford, W. M., Geldart, L. P., and Sheriff, R. E., 1990, Applied Geophysics, 2nd ed.: Cambridge University Press